Reverse Self-Assembly: (111)-Oriented Gold Crystallization at Alkylthiol Monolayer Templates

Ahmet Uysal,[1] Benjamin Stripe,[1] Binhua Lin,[2] Mati Meron,[2] and Pulak Dutta[1]

[1]*Department of Physics and Astronomy, Northwestern University, Evanston, Illinois 60208, USA*
[2]*Center for Advanced Radiation Sources, The University of Chicago, Chicago, Illinois 60637, USA*

(Received 17 June 2011; published 8 September 2011)

It has long been known that thiol-terminated molecules self-assemble as commensurate monolayers on Au(111) surfaces. By spreading floating octadecanethiol monolayers on aqueous solutions of chloroauric acid ($HAuCl_4$) and using x rays to reduce the gold ions as well as to probe the structure, we have observed the nucleation of (111)-oriented Au nanoparticles at thiol surfaces. This process may be similar to the formation of biogenic gold by bacteria. The thiol monolayer acts as a ''soft template,'' changing its structure as Au crystals form so that there is a $\sqrt{3} \times \sqrt{3}$ commensurate relationship.

DOI: 10.1103/PhysRevLett.107.115503 PACS numbers: 81.10.Dn, 82.65.+r, 87.64.Bx

The self-assembly of organic molecules on metal or oxide surfaces offers a simple and flexible way of controlling surface properties, for a wide range of applications from organic electronics to wetting and adhesion [1]. On the other hand, biomineralization is an important area of research with potential applications to functional material fabrication methods in ambient (''mild'') conditions [2]. The methods used by living organisms to precisely control the orientation of inorganic nanocrystals in biominerals, and thus to build organic-inorganic composite structures with enhanced mechanical and optical properties, is still poorly understood [2]. These two processes (self-assembly and biomineralization) are in some sense reciprocal to each other, and both are driven by interactions at the organic-inorganic interface. We have combined aspects of these fields to grow gold nano- or microparticles from solutions. Using synchrotron x rays, we see that the organic monolayer and gold surface lattices are commensurate, resulting in a predominantly (111) orientation of the gold crystals. These results show how ideas from apparently disparate research areas can be used to develop new and better ways to make tailored nanomaterials.

Many studies [3] have demonstrated the ability of microorganisms to reduce Au^{3+} ions present in water as chloroauric acid and to grow gold nano- or microparticles in a controlled way. Reith *et al.* [4] showed that the formation of Au(I)-S complexes is an intermediate stage during nucleation of gold by bacteria. On the other hand, So *et al.* [5] showed that it is possible to engineer new peptides with a higher affinity to Au(111), attributed to a geometrical match between the peptide and the gold surface. It is, of course, well known that alkylthiols self-assemble on Au(111) with an organic-inorganic lattice match [6]. Thus the two key concepts of epitaxy and high affinity of sulfur to gold are relevant both to organic-directed gold crystallization and to the self-assembly of alkylthiols on gold surfaces. This suggests that monolayers of alkylthiols may be the perfect template to grow (111)-oriented, anisotropic, gold nano- or microparticles in ambient conditions.

Floating (Langmuir) monolayers of organic molecules have been used widely for model biomineralization studies [7,8] because of their similarities to biological membranes and because the water surface is easily accessible to various experimental probes. For this study they have the additional advantage of being two-dimensional, which leads to anisotropic crystal morphologies, often a desired property for functional nanoparticles [9]. Langmuir monolayers or Langmuir-Blodgett films have been used in recent studies to grow gold nanoparticles at the air-water interface or in constrained environments [10–13]. In some of these studies Au^{3+} ions were reduced spontaneously to form metallic gold particles [10,11], while in other cases organic molecule-gold ion complexes were transferred to solid substrates and then reduced by using UV radiation [12,13]. Some other organic templates, combined with x-ray photoreduction, have also been used for controlled gold nanoparticle growth experiments [14,15]. However, in all these cases the crystals were either unoriented, or orientation was studied only for crystals transferred from water surfaces to hard substrates (a process that orients platelike crystals even if they were not oriented before transfer). None of the above studies obtained *in situ* information about the organic-gold interface structure.

Self-assembled monolayers (SAMs) of alkylthiol on solid and liquid metal surfaces have been studied extensively [1,16,17]. They can also form floating monolayers on water [18,19], but these have attracted little attention. The thiol (SH) headgroup cannot form strong hydrogen bonds with water, and so the monolayer is less stable than those with more hydrophilic headgroups. Previous studies with Brewster angle microscopy [18] and ellipsometry [19] showed coexistence of monolayers with thicker structures on pure water and on subphases with metal ions. However, no x-ray studies have been conducted to determine the exact structures, nor have any experimental results been previously reported about alkyl thiol monolayers on chloroauric acid solutions.

In this study of gold crystallization under octadecanethiol (C18S) Langmuir monolayers at the air-water interface, we used *in situ* grazing-incidence x-ray diffraction (GID) to probe organic monolayer structure and gold particle surface structures simultaneously. Besides being a powerful probe to study the organic-inorganic interface, synchrotron x rays also acted as a reducing agent in this experiment. Figure 1 shows our experiment in schematic form. We spread Langmuir monolayers of C18S from chloroform solution on 6 mM chloroauric acid subphases at room temperature. We compressed and kept the monolayer at a constant surface pressure of 10 mN/m. We turned on the x-ray beam ~1 h after the monolayer was prepared. Synchrotron GID experiments were conducted at Sector 15ID, ChemMatCARS of Advanced Photon Source. The monochromatic x-ray beam had an energy of 10 keV ($\lambda = 1.240$ Å). The beam footprint had dimensions of 1 mm × 9 cm, which is less than 1% of the total Langmuir monolayer area. In the grazing-incidence geometry, the x-ray penetration depth is of the order of 10^{-8} m, so that photoreduction is limited to the air-water interface along the beam footprint. We used a Pilatus 100 K pixel array detector at pinhole mode for quick and accurate data acquisition. Details of the experimental setup and utilization of the Pilatus detector at pinhole mode have been reported previously [20–22]. We also repeated the experiments at sector X14A of National Synchrotron Light Source to confirm that the results were not artifacts of the setup or the beam. We transferred gold crystals from the air-water interface onto TEM grids and silicon substrates for *ex situ* imaging. A Hitachi-8100 TEM and a Hitachi-S3400 scanning electron microscope were used to image nano- and microstructures, respectively.

Figures 2(a) and 2(b) show GID intensity contours of the (111)-oriented gold crystals. The peaks appear after ~15 min from the start of the radiation and get stronger with time [Fig. 2(c)]. The in-plane peak at (Q_{xy}, Q_z) coordinates of (4.36, 0) Å^{-1} is the $(\bar{2}20)$ peak of Au [Fig. 2(b)], which is normal to the (111). The off-plane peak at (2.52, 0.90) Å^{-1} is 20° above the horizontal [Fig. 2(a)], and it is the Au $(1\bar{1}1)$ peak, which is 70° away from the (111). These results establish that the scattering is from (111)-oriented gold crystals. These data represent an ensemble average of crystals in a macroscopic region over the x-ray beam footprint (~ 1 cm^2). The time evolution of the one-dimensional diffraction peak derived from the GID contour of $(\bar{2}20)$ indicates the increase of number and/or size of gold particles with time [Fig. 2(c)]. The faint signal observed along the Debye rings [particularly visible in Fig. 2(b)] indicates the formation of some unoriented particles.

TEM images of gold crystals at the early stages show the formation of platelike hexagonal gold nanoparticles with size ~50 nm [Fig. 3(a)]. These nanoparticles merge and/or grow to form micron-size gold microplates [Fig. 3(b)]. In the very late stages, flowerlike particles start to form [Fig. 3(c)]. However, it is still possible to see the hexagonal platelets at the base of the "flower." Interestingly, some electrochemical fabrication methods lead to similar gold particle morphologies [23], but a detailed investigation of these mature structures is beyond the scope of this Letter.

We now turn to the structure of the organic template. The intensity contours of GID data in Figs. 4(a)–4(c) show all peaks observed from the C18S structure. The data collected in the $Q_{xy} = 1.39$–1.55 Å^{-1} region are plotted as collected after 10 min [Fig. 4(a)] and after 100 min [Fig. 4(b)] to show the changes with time (before and after gold crystals have formed). The in-plane peak ($Q_z \approx 0$) at

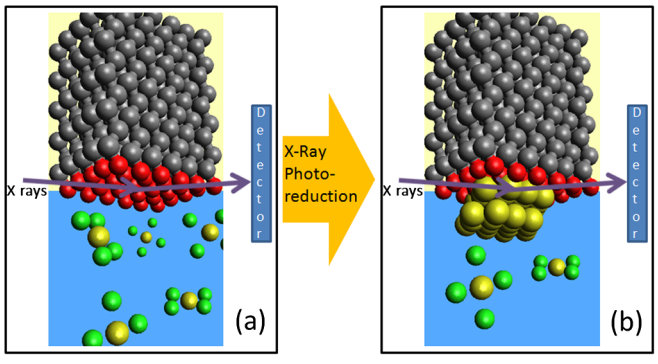

FIG. 1 (color online). A representation of our "reverse self-assembly" experiment at the air-water interface. (a) The upper half of each frame shows a floating monolayer formed by spreading octadecanethiol on an aqueous solution of $HAuCl_4$. (b) The synchrotron beam produces elemental gold by photoreduction and is also used to characterize the resulting gold crystals through diffraction.

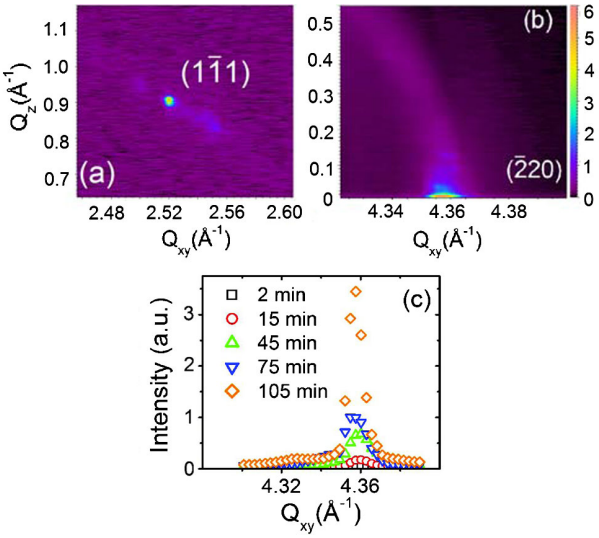

FIG. 2 (color online). (a),(b) *In situ* GID intensity contours of gold crystals. The peak positions confirm that the gold particles are (111)-oriented. (c) Time resolved one-dimensional diffraction scans derived from $(\bar{2}20)$ peak in (b). Data are integrated over $Q_z = 0.02$–0.04 Å^{-1}.

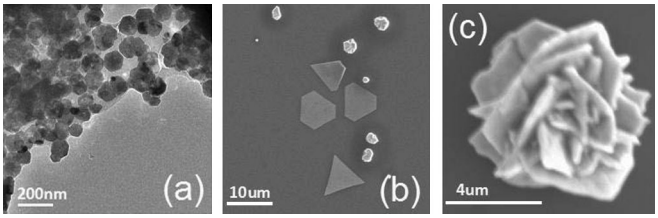

FIG. 3. Electron micrographs of gold crystals collected from the air-water interface. (a) TEM micrograph after ~20 min. (b),(c) Scanning electron microscope micrographs after 2 and 4 h, respectively. It is possible to see the hexagonal plate at the base of the flowerlike particle in (c).

$Q_{xy} = 1.69$ Å^{-1} [Fig. 4(c)] does not move with time; it is shown only once. One-dimensional diffraction scans derived from the contour scans [Figs. 4(d)–4(g)] help us to calculate the exact position and width of the peaks. The coordinates of the peaks in the (Q_{xy}, Q_z) plane tell us the structure of the monolayer in the plane of the water surface, as well as the tilt magnitude and direction [24]. We also study the vertical Bragg rod (BR) profiles of the peaks to calculate the thickness of the layers. The half width at half maximum (Δq_z^{BR}) of a BR is inversely proportional with the layer thickness $d^{\mathrm{BR}} \sim \pi/(\Delta q_z^{\mathrm{BR}})$ [16]. Similarly, the correlation length (ξ) of a laterally ordered layer is inversely proportional to the width of its GID peak.

At 10 min there are at least three peaks originating from the alkyl chains of the C18S molecules: two in-plane peaks at $Q_{xy} = 1.69$ and 1.51 Å^{-1} and a broad off-plane peak ($Q_z \neq 0$) at $Q_{xy} = 1.40$ Å^{-1}. The vertical profile of the 1.51 Å^{-1} peak [Fig. 4(e)] has two different slopes, indicating that it is actually a combination of a short BR ($\Delta q_z^{\mathrm{BR}} = 0.14$ Å^{-1}) and a long BR ($\Delta q_z^{\mathrm{BR}} = 0.63$ Å^{-1}). The short BR corresponds to a monolayer ($d^{\mathrm{BR}} \sim 23$ Å), and the long BR indicates the existence of a thinner layer ($d^{\mathrm{BR}} \sim 5$ Å) with the same lateral order but significantly different electron density than the alkyl chains.

The BR of the peak at 1.69 Å^{-1} is less wide [Fig. 4(g)] and indicates a thickness of ~40 Å, which corresponds to a bilayer of C18S. The presence of bilayers has been reported previously based on ellipsometry and isotherm studies [18,19]. Considering the number of molecules spread and the monolayer area, the bilayer structures cannot cover more than a small fraction of the surface. Also, the bilayer peaks do not move during the experiment, indicating that they do not interact with the gold significantly.

We interpret the shape of the off-plane peak at $Q_{xy} = 1.40$ Å^{-1} [Fig. 4(f)] as overlapping monolayer and bilayer peaks. The presence of an off-plane monolayer peak indicates that the monolayer is titled, as is reasonable for such an expanded structure. The calculated tilt is ~30°, a common tilt for alkane chains [17] and also similar to that of a Langmuir monolayer of C18S on mercury [16]. In the

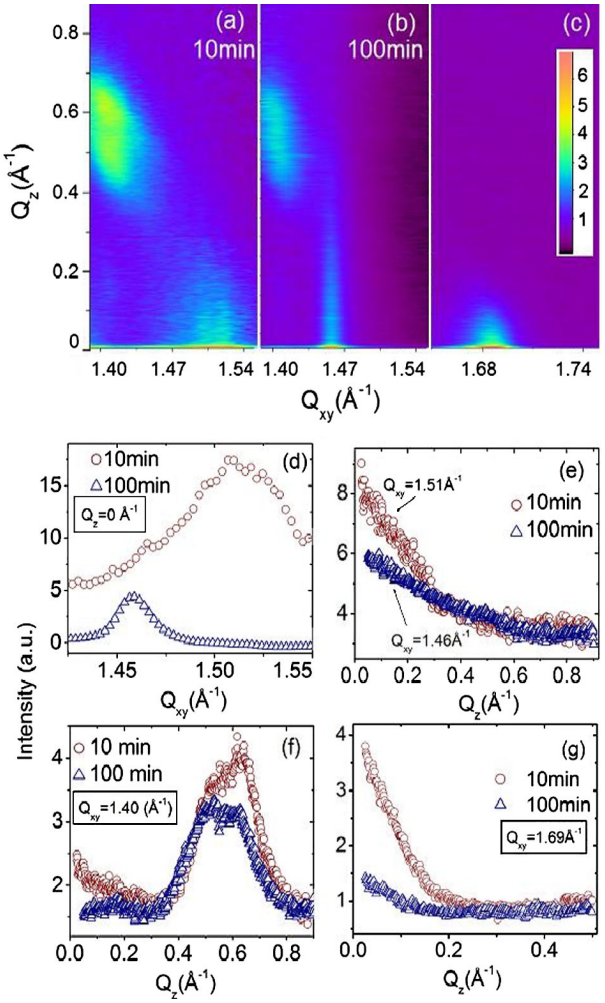

FIG. 4 (color online). (a),(b) *In situ* GID intensity contours of octadecanethiol peaks at two different times, before and after gold crystals formed. (c) Peak due to the molecular bilayer, which does not move with time. (d)–(g) One-dimensional diffraction scans derived from the intensity contours. Data are integrated over $Q_z = 0.02$–0.04 Å^{-1} for the horizontal scan (d) and $\Delta Q_{xy} = \pm 0.01$ Å^{-1} around the given Q_{xy} value for the vertical scans (e)–(g). The data for 10 and 100 min have different scales for better visibility, in all plots except (d).

early stages, therefore, the structure of the C18S monolayer is determined completely by the van der Waals interactions between the alkyl chains. This situation is a result of the weak hydrophilicity of the thiol headgroup. This structure can be contrasted to the SAMs on Au(111) [1,6,17] and Langmuir monolayers of C18S on mercury [16], where strong headgroup-substrate interactions play a significant role on the monolayer structure.

The ~5 Å thick layer with significantly different electron density than the tails cannot be attributed to −SH headgroups only because their electron density would not be high enough to be distinguishable from the tail groups. Therefore, we conclude that the thiol headgroups form a complex with gold ions in the subphase.

Unlike spectroscopic measurements [25], GID cannot determine the chemical state of the components, but gold ions are the only component of our fairly simple system with such high electron density. RS-metal-SR [where $R = (CH_2)_nCH_3$] complexes have been observed in thiol SAMs deposited on Au(111) [26] and in C18S monolayers on mercury [16], and Au(I)-S complex formation is also reported during biomineralization of gold by bacteria [4]. The 1 h time scale is similar to the time required for silver complex formation with C18S Langmuir monolayers on aqueous $AgNO_3$ solution [19].

Although the structure of the C18S monolayer is interesting in itself, for the purposes of this Letter, the more relevant result is the new monolayer structure after 100 min (when gold crystals have formed). The original monolayer in-plane peak disappears, the bilayer peaks weaken, and a new in-plane peak appears at $Q_{xy} = 1.46$ Å^{-1} [Fig. 4(b)]. This new peak has a long BR that corresponds to a ~5 Å thickness [Fig. 4(e)]. That is the only peak attributable to a monolayer in the late stages. Therefore, we conclude that this new structure is a hexagonal lattice: The lattice parameters are $\mathbf{a} = 4.99$ Å and $\mathbf{b} = 8.64$ Å in the centered rectangular unit cell convention ($b/a = \sqrt{3}$). This structure corresponds to a $\sqrt{3} \times \sqrt{3}R30°$ superlattice on the Au(111) surface and is the same as that observed with alkylthiol-Au(111) SAMs [6]. It should be noted that, although the initial correlation length (ξ) of the monolayer is ~70 Å, the sharper peak at $Q_{xy} = 1.46$ Å^{-1} gives $\xi > 300$ Å. This length scale nicely matches with the size of the nanoparticles that we observed with electron microscopy [Fig. 3(a)]. The vanishing of the alkyl tail peaks at 1.40 and 1.51 Å^{-1} with time shows that, during the reorganization of the headgroups to match the gold surface structure, the in-plane order of the tail groups is weakened or lost. The presence of water molecules, as well as the different route through which the SAM-gold assemblies are formed, may cause subtle structural differences between SAMs deposited on Au(111) substrates [1,6,26,27] and our system.

These results show the advantages of a "soft" adaptable template for oriented crystallization, as well as the importance of epitaxy. Chain-chain van der Waals interactions determine the floating monolayer structure before crystallization. However, that structure is close enough to the Au(111) surface structure to adapt itself to the growing gold surface. Of course, while the monolayer structure can change, the monolayer orientation is fixed by the water surface, and thus template adaptability promotes the growth of oriented gold nanoparticles. This can be compared to the biomimetic crystallization of other minerals at the water surface, where both organic and inorganic structures change to lower the interface potential energy [22,28].

In summary, we have "reversed" a well-known self-assembly process to grow oriented, anisotropic gold nanoparticles and monitored the hard-soft interface structure *in situ*. These experiments suggest that the vast body of knowledge in the molecular self-assembly field can be utilized to develop new pathways for the manufacture of designed nanomaterials.

We thank Kyungil Kim and Jianming Bai for their advice and assistance in synchrotron experiments. This work was supported by the U.S. National Science Foundation under Grant No. DMR-1006432. ChemMatCARS Sector 15 is principally supported by the NSF/DOE under Grant No. NSF/CHE-0822838. Beam Line X14A, Advanced Photon Source, and National Synchrotron Light Source are supported by the U.S. DOE. The electron micrographs were recorded at Electron Probe Instrumentation Center, Northwestern University.

[1] J. C. Love *et al.*, Chem. Rev. **105**, 1103 (2005).
[2] S. Mann, *Biomineralization: Principles and Concepts in Bioinorganic Materials Chemistry* (Oxford University, New York, 2001).
[3] K. B. Narayanan and N. Sakthivel, Adv. Colloid Interface Sci. **156**, 1 (2010).
[4] F. Reith *et al.*, Proc. Natl. Acad. Sci. U.S.A. **106**, 17 757 (2009).
[5] C. R. So *et al.*, ACS Nano **3**, 1525 (2009).
[6] P. Fenter, P. Eisenberger, and K. S. Liang, Phys. Rev. Lett. **70**, 2447 (1993).
[7] A. Dey *et al.*, Nature Mater. **9**, 1010 (2010).
[8] E. DiMasi *et al.*, Phys. Rev. Lett. **97**, 045503 (2006).
[9] M. A. El-Sayed, Acc. Chem. Res. **34**, 257 (2001).
[10] Z. H. Xue *et al.*, Mater. Chem. Phys. **123**, 278 (2010).
[11] S. Kundu and A. Das, Chem. Phys. Lett. **508**, 80 (2011).
[12] S. Ravaine *et al.*, Langmuir **14**, 708 (1998).
[13] F. W. Hsiao, Y. L. Lee, and C. H. Chang, Colloids Surf. B **73**, 110 (2009).
[14] F. Karadas *et al.*, Langmuir **21**, 437 (2005).
[15] Q. Ma *et al.*, Appl. Phys. Lett. **76**, 2014 (2000).
[16] B. M. Ocko *et al.*, Phys. Rev. Lett. **94**, 017802 (2005).
[17] A. Ulman, Chem. Rev. **96**, 1533 (1996).
[18] M. Broniatowski, J. Colloid Interface Sci. **337**, 183 (2009).
[19] W. Z. Zhao *et al.*, Langmuir **12**, 386 (1996).
[20] M. Meron *et al.*, Eur. Phys. J. Special Topics **167**, 137 (2009).
[21] B. H. Lin *et al.*, Physica (Amsterdam) **336B**, 75 (2003).
[22] A. Uysal *et al.*, CrystEngComm **12**, 2025 (2010).
[23] G. T. Duan *et al.*, Appl. Phys. Lett. **89**, 211905 (2006).
[24] V. M. Kaganer, H. Mohwald, and P. Dutta, Rev. Mod. Phys. **71**, 779 (1999).
[25] M. Prato *et al.*, J. Phys. Chem. C **112**, 3899 (2008).
[26] A. Cossaro *et al.*, Science **321**, 943 (2008).
[27] E. Torres, A. T. Blumenau, and P. U. Biedermann, Chem. Phys. Chem. **12**, 999 (2011).
[28] J. Kmetko *et al.*, Phys. Rev. Lett. **89**, 186102 (2002).